We are IntechOpen, the world's leading publisher of Open Access books
Built by scientists, for scientists

6,900
Open access books available

185,000
International authors and editors

200M
Downloads

Our authors are among the

154
Countries delivered to

TOP 1%
most cited scientists

12.2%
Contributors from top 500 universities

CLARIVATE ANALYTICS
BOOK CITATION INDEX
INDEXED

WEB OF SCIENCE™

Selection of our books indexed in the Book Citation Index
in Web of Science™ Core Collection (BKCI)

Interested in publishing with us?
Contact book.department@intechopen.com

Thin-Film Solar Cells Performances Optimization: Case of Cu (In, Ga) Se$_2$-ZnS

Fridolin Tchangnwa Nya and Guy Maurel Dzifack Kenfack

Abstract

In this chapter, we investigate a way of improving solar cells performances. By focusing studies on optimizing the structural, the opto-electrical and electronic properties of materials that constitute the layers and interfaces of a solar device, such as electrical susceptibility, doping concentration, mobility of charge carriers and crystallographic structure, it is possible to improve the output parameters of a solar cell. Working on a CIGSe-based second-generation ultra-thin solar cell model, and using Zinc Sulfide (ZnS) as a window layer, and based on recent studies, vital information are found on the optimal values of these properties that may enhance the efficiency of the cell. A correct modeling of the device with a trusted software such as SCAPS and an appropriate set of the exact conditions and parameters of simulation allow to obtain very promising results. In particular, for nanoscale and microscale thicknesses of buffer and absorber layers materials respectively, and with an appropriate choice of other materials properties such as intrinsic doping concentration, electrons and holes mobilities, it is possible to record efficiencies and fill factors of more than 26% and 85% respectively. These values are very promising for solar energy harvesting technologies development through CIGSe – ZnS based solar devices.

Keywords: thin-film, solar cell, CIGSe, ZnS, efficiency optimization, SCAPS numerical simulation, structural properties, Opto-electrical properties

1. Introduction

These two last decades have been marked by a dizzying rise in the field of solar energy harvesting thanks to photovoltaic technologies. Among the three well-known fields of solar device technologies, thin-film solar cells are nowadays gaining more interest among researchers and industrial applications due to the reduction in the quantities of materials, their flexibility, their low environmental impact, reduction in time and new opportunities for higher yields goals. The achievement of a record yields of 22.6% [1] for CIGSe-based thin-film solar cells at the end of 2016 marked a decisive turning point towards the quest for higher yields. On the basis of recent studies, the efficiency of CIGSe-based ultra-thin solar cells can be further considerably improved by directing studies on obtaining the best structural and opto-electrical properties of the different materials layers that constitute the cell structure. For example, among the alternative materials for the buffer layer, scientific community recognizes the Zinc Sulfide ZnS material as the one which stands

out as the most promising, although the highest yield obtained with it to date does not exceed 22%. In the process of reducing the thickness of the layers, numerous works have been identified. In 2015 a yield of about 20.75% was achieved with CIGSe device using only 1 μm of absorber layer thickness and ZnS as buffer layer [2]. A couple of years later, a yield of 22.62% is recorded using nanoscale thicknesses for the different layers but using the controversy CdS material as buffer layer [3]. By going into continuation of the above-mentioned works, a correct modeling with the trusted numerical simulation software SCAPS allow to investigate the influence of the values of certain properties of layers and interfaces mainly, their electrical susceptibility, their crystallographic structure, their intrinsic doping level and the mobilities of charge carriers, on the performances of CIGSe-ZnS based solar cell structures. In this chapter, we carry out investigations and we highlight key properties values that allow to record very promising results. A good knowledge of these values is a basis to better control the material design and layers deposition processes, to be closed to these theoretical results [4, 5]. To achieve this goal a good understanding of the micro-activities which occur at the level of the layer interfaces which are the recombination mechanisms of the photo-generated electron-hole pairs, and the effects of the defect states which inevitably appear with thicknesses reduction, is required to limit their harmful effects on the cell performances [6, 7].

This chapter will be structured as follow, in the first section we are presenting the state of the art on CIGSe-based second-generation thin film solar cells. The different properties of materials are highlighted in the second section, and we recall the mathematical relationships that support the microscopic phenomena within layers and interfaces, and which constitute the basis set of our solar cell modeling. In the last section, investigations are carried out to understand the influence of certain material properties on the overall performance of our device and depending on the results obtained, we highlight those which lead to better yields.

2. State of the art on solar cells - introduction on CIGSe-based thin films

2.1 State of the art in thin film industry

The photovoltaic market has experienced rapid development since 2003, with a growth rate of 40% until 2009 and 135% in 2010, reaching an installed capacity of 40 GW. This market is dominated by technologies based on crystalline silicon. Developed for 60 years, the silicon industry witnessed many advances. In 2012, it represented 90% of the photovoltaic market share [8]. We can then distinguish two large families of cells depending on the nature of the silicon wafer, monocrystalline (m-Si) or poly crystalline (p-Si), for which the record yields are 26.8% (homo-junction), 24.9% (heterojunction) and 21.7% (homojunction), 20.3% (heterojunction) respectively [9]. Research in this field has been extremely active in recent years and advances have been rapid, which has allowed the advent of photovoltaic technologies that consume less energy and only require a few microns in thickness (compared to around 200 microns for silicon) and costs of smaller productions. This is the so-called second generation thin-film cell industry. Their main advantage comes from the small amount of materials needed to make a cell. This generation experienced a 39% increase in production between 2010 and 2014 and more than 50% between 2015 and 2019. There are mainly three (03) sectors in that field:

- **Amorphous silicon (a-Si) thin films**: they have record efficiencies of around 11% for single junction amorphous silicon cells and 12.6% for tandem double junction amorphous silicon/micro-amorphous silicon cells.

- **Cadmium Telluride (CdTe) thin films**: the record yield is 22.1%. It is the leading thin film technology in the photovoltaic industry. However, a promising future is not guaranteed because of the use of cadmium (Cd) which is a highly harmful material for environment purpose.

- **Thin films based on Indium Gallium Copper DiSelenide Cu (In, Ga) Se$_2$**, known as CIGSe based solar cells: which represent the best yields with a conversion yield of 22.6% in 2016 [1].

The third generation includes all the new approaches proposed and developed in recent years, this generation is to reduce manufacturing costs (Organic solar cells, Gräetzel[1] cells, etc.). It seeks to overcome the current limits of yields by resorting to original concepts such as multi-junction cells, intermediate gap cells or using hot carriers. The majority of third generation systems are currently under development and target more or less long-term industrial applications. Gräetzel cells for example can offer a yield of up to 11.5% [1].

2.2 CIGSe-based cells: evolution

The scientific advances which have enabled the realization of very high efficiency thin film solar cells have taken place by successive technological leaps, the study of these different key stages is essential to understanding the complexity of the structure of a solar cell based on standard CIGSe and the problematic of this work.

Initially intended for the manufacture of photo-detectors, the first solar cells consisted of single crystals of CuInSe$_2$ (CISe) evaporated on an alumina/molybdenum substrate. Interest in photovoltaic applications grew very quickly in regards to the good yields of around 9% obtained by BOEING in 1981. Since the 1980s, four main developments have made it possible to obtain current yields.

- *Modification of the structure*

Modification of the buffer layer by the Cadmium Selenide (CdS) layer and the introduction of the ZnO: Al window layer enhanced absorption of the solar spectrum at short wavelengths. As of today, many materials have already been used as a buffer layer in particular (In$_2$S$_3$, ZnS, ZnSe, Zn (S, OH)) and as a window layer we will see for example zinc oxide doped with Boron (ZnO: B).

- *Introduction of Gallium*

Beginning in 1987, Chen et al. [9] attempted to incorporate Gallium atoms into the CISe structure. The partial substitution of indium by gallium has improved the electrical performance of the solar cell.

- **Influence of sodium**

In the 1990s, Hedson et al., working on the substitution of the initial substrate to soda glass in order to reduce costs, found that the performance of solar cells was

---

[1] It was in 1991 that Gräetzel's cell was discovered by Michael GRÄETZEL, a Swiss chemist and professor at the Swiss Federal Institute of Technology in Lausanne.

greatly improved. They attributed this observed beneficial effect to the influence of sodium from the glass on the doping of the CIGSe layer.

- **Filing procedures**

The importance of the deposition processes of the absorbent layer was studied in the Boeing laboratory, going from one to two, then to three stages, the deposition processes have made it possible to improve the performance of solar cells by various phenomena. That are the burial of the P-N junction, the Gallium gradient and recrystallization.

2.3 Challenges to take up

Advances in the field have enabled CIGSe based technology to exceed the 20% yield recorded in 2010 and yields close to 23% in 2016. If this technology is actually offering very good yields for thin films structures, it is also facing many economic, environmental and competitive challenges strongly linked to this last decade requirements.

- **The first challenge: Reducing production costs**.

The European Union has classified Indium as a critical material since 2010 due to the drastic lowering of its reserves following its multi-field use where demand is increasingly growing in addition to the photovoltaic market (ITO screen, LED, etc.) and the instability of its cost is already hindering the development of CIGSe technology. Among the distinct avenues of research aiming at reducing the use of Indium, the reduction of the thickness of the CIGSe layer is the subject of this work.

- **The second challenge: Reducing the environmental impact, replacing the buffer layer with a less harmful layer**.

Known CIGSe-based cell models use Cadmium Sulfide (CdS) as the buffer layer material. The latter has so far provided the best returns. However, the cadmium present in the material is a highly carcinogenic element representing a potential danger during the manufacturing and recycling phase at the end of the lifetime.

- **The third challenge: Obtain better performance and compete with other technologies.**

So far, the record performance achieved by CIGSe-based thin-film photovoltaic technology is 22.6% [1], close to the highest yield of 24.9% recorded by silicon technology. The main goal of the present development, is to undertake scientific investigations to go beyond the above-mentioned values.

2.4 Thin film issue

In principle, a thin layer of a given material is an element of this material, one of its dimensions, called the thickness, has been greatly reduced so that it is expressed in nanoscale and that this small distance between the two boundary surfaces (almost two-dimensionality) leads to a disturbance of the majority of the physical properties.

The second essential characteristic of a thin film is such that whatever the procedure used for its manufacture; a thin film is almost part of the support on

which it is built. Consequently, the support has a very strong influence on the structural properties of the layer deposited thereon.

Much work already exists in the context of optimizing the performance of CIGSe cells with various materials as a buffer layer. It is in this tertiary perspective that this work is also part of, that is to say to seek the optimized properties of the material used as a buffer layer and to control the micro-activities behind performance losses.

3. Material choosing, methods and general principle

3.1 Material choosing and structure of our solar cell

3.1.1 Reason for choosing ZnS

Zinc Sulfide (ZnS) is a semiconductor formed by the association of an element atom from column II with another element atom from column VI of the periodic table of chemical elements. It has intrinsic properties which make it a material of choice in the search for good performance in the CIGSe-based thin film chain. It is recognized as having the following properties: It is non-toxic to the environment and its constituents are abundant in nature (Zinc and Sulfur) (**Table 1**).

3.1.2 ZnS material global properties

3.1.2.1 ZnS crystallographic properties

The crystallography of compounds II-VI6 to which Zinc Sulfide belongs poses some problems because of the polymorphism of these compounds. They can have crystallographic structures of two main types: the cubic structure of the sphalerite type (Zinc Blende), and the hexagonal structure of the Wurtzite type. The cubic structure (Zinc Blende) is stable at room temperature (27°C), while the hexagonal structure is more stable at very high-top temperatures of around 1020°C [10]. Indeed, with a lattice parameter $a_{CIGS} = 0.58\ nm$ for the CIGSe chalcopyrite structure and $a_{0\_ZnS} = 0.541\ nm$ respectively $a_{0\_ZnS} = b_{0\_ZnS} = 0.3811nm$ for ZnS in its cubic and hexagonal structure respectively, CIGSe forms a better lattice agreement with ZnS in its sphalerite structure which is furthermore its stable structure [11].

A deposition technique by ALD [12] or by laser sputtering [11] would make it possible to obtain a layer of ZnS having a crystallographic orientation preferentially sphalerite.

Column I A-B	Column II A-B	Column III B	Column IV B	Column V B	Column VI B	Column VII B
Li$_3$	Be$_4$	B$_5$	C$_6$	N$_7$	O$_8$	F$_9$
Na$_{11}$	Mg$_{12}$	Al$_{13}$	Si$_{14}$	P$_{15}$	[S$_{16}$]	Cl$_{17}$
Cu$_{29}$	[Zn$_{30}$]	Ga$_{31}$	Ge$_{32}$	As$_{33}$	Se$_{34}$	Br$_{35}$
Ag$_{47}$	Cd$_{48}$	In$_{49}$	Sn$_{50}$	Sb$_{51}$	Te$_{52}$	I$_{53}$
Au$_{79}$	Hg$_{80}$	Ti$_{81}$	Pb$_{82}$	Bi$_{83}$	Po$_{84}$	At$_{85}$

Table 1.
Chemical elements of the Mendeleev table of columns II and VI [13].

3.1.2.2 ZnS Opto-electrical properties

The spectrum of white light extends from the ultraviolet characterized by short wavelengths ($\lambda < 380$ nm) to the infrared characterized by long wavelengths ($\lambda > 780$ nm) through the visible spectrum whose wavelengths are between 380 nm $< \lambda < 780$ nm. The absorption spectrum of ZnS is an important element that characterizes its absorption power when subjected to illumination. It is all the more significant as it extends over a frequency band that is difficult to absorb by other materials. The important element to characterize it is the value of the band gap of the material. The energy value of the band gap, E_g of ZnS can be determined by an optical approach through its absorption spectrum. The formula that describes light absorption ability of a material given his band gap is well highlighted by Rayan, Elseman and co-workers [14–16] and is given by:

$$(\alpha h \nu)^2 = A\left(h\nu - E_g\right) \tag{1}$$

This formula is only valid for authorized direct transitions. α is the absorption coefficient, A is a constant to be determined, $\hbar$ is Planck's constant and ν is the frequency of the incident photon.

Literature tells us that ZnS is a semiconductor with a wide band gap (> 3.5 eV). This wide band gap gives it high optical transparency in the visible and infrared regions of the solar spectrum and a high absorption coefficient in the ultraviolet region. Its transmission spectrum is recorded between 400 and 850 nm [17], which allows the transmission of photons of higher energy, thus increasing the absorption of the light spectrum in the absorber layer.

It is also a direct gap semiconductor. Indeed, the maximum of the valence band and the minimum of the conduction band are found at the centre of the Brillouin zone (where $\vec{K} = 0$). The transitions are made from band to band without the intervention of phonons, therefore without loss or dissipation of energy in thermal form [18].

The refractive index of ZnS is 2.41 to 0.5 μm and 2.29 to 1.1 μm in depth [19]. Remember that the electronic structures of Sulfur and Zinc are:

$$Zn : [Ar]4d^{10}5s^2 \quad S : [Ne]3d^2 3p^4$$
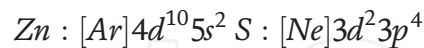
The $3p$ states of Sulfur form the valence band, the $5s$ states of Zinc constitute the conduction band. This gives ZnS a wide forbidden band. This wide band gap makes it a very promising material for optoelectronic and solar applications. Its forbidden band is between 3.68 eV and 3.9 eV depending on whether we are in a cubic or hexagonal structure. This band gap value may vary depending on the preparation method and the doping rate [19]. We can also find from the literature that it has a relatively high exciton binding energy ($34\ meV$); its structure exhibits a better lattice matching with absorbers having energy bands in the range ($1,2–1,5\ eV$) [13] and finally it has a high electrons mobility ($165\ cm^2/V.\,s$).

3.1.3 Structure of our solar cell

In its most common structure, a CIGSe-based cell is formed by a stack of several thin film materials deposited successively on a substrate. Let us consider the following structure:
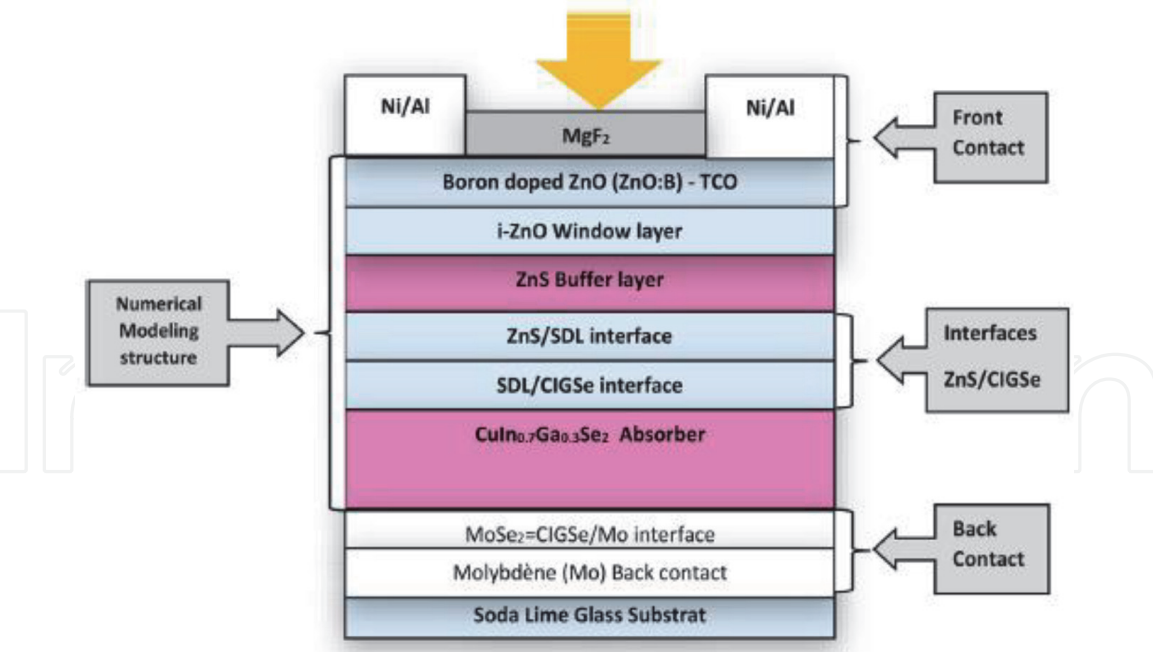(Ni/Al)/MgF2/ZnO: B/i-ZnO/ZnS/CuInGaSe$_2$/Mo/SLG (**Figure 1**).

Figure 1.
One-dimensional structure of the cell.

- **Second window layer: i-ZnO**

Zinc oxide is a semiconductor belonging to group II-VI with a number of properties that make it a material widely used in several fields, these are its piezoelectricity, its wide band gap and its intrinsic doping type N. It can exhibit an N-type doping process, for example by adding the atoms of Al, Ga and B and it also exhibits an N-type conductivity due to structural defects. Its forbidden band is 3.3 eV and can vary by adding Mg, Cd or S atoms. It can crystallize according to the Zinc Blende, wurtzite or diamond structures. Only the wurtzite structure is stable under ambient conditions [20].

- **First window layer: ZnO: B**

Most CIGSe-based solar cells use Aluminum-doped Zinc oxide (ZnO: Al) as the Transparent Conductive Oxide (TCO). Within the framework of this work we opt for ZnO doped with boron (ZnO: B) as OCT. Boron doping would be more beneficial for solar cells. Its standard thickness varies between 450 and 1400 nm [18].

- **The buffer layer: ZnS**

Its standard thickness varies between 40 and 60 nm. It has an N-type conductivity and its gap is greater than that of the absorber layer. Three roles are mainly attributed to it:

- **An electrical role**: it adapts the width of the forbidden band between the absorber and the window layer and limits the recombination of carriers at the interface;

- **An optical role**: due to its wide forbidden band (E_g = 3.68 eV), it makes it possible to absorb the maximum of the light spectrum in the region not absorbed by the active layer and thus minimizes optical losses;

7

- **A role of protective layer**: it protects the surface of the absorber during the deposition of the ZnO layer, which can cause defects on the surface of the CIGSe.

From Won Song et al. work [19], only the values of properties recorded for the cubic structure will be taken into account during this study, since that structure is more stable at room temperature, and forms a better lattice matching with the chalcopyrite structure of CIGSe. That allows us to record as dielectric constant value $\varepsilon_r = 8.3$.

- **The absorbent layer: Cu (In, Ga) Se$_2$**

It is a semiconductor obtained by combining elements from groups I-III-VI2 of the periodic table (**Table 2**) and has a chalcopyrite crystal structure. Its standard thickness is between 1.5 - 3 μm. This tetragonal structure can be described as a stack of two Zinc Blende structures in which the tetrahedral sites are occupied by atoms of group VI (Se) (anions) and the other sites are occupied in an orderly manner by atoms of groups I (Cu) and III (In) (cations). CIGSe is a solid solution of the semiconductor materials CuInSe$_2$ and CuGaSe$_2$ which have direct gaps of 1.06 eV and 1.7 eV respectively.

$$\text{The ratio} : x = \frac{[Ga]}{[Ga] + [In]} \tag{2}$$

determine the rate of Gallium atoms that replace Indium atoms in the structure. The value of the band gap and the electrical susceptibility of the material vary as a function of x between the values of pure CIS and pure CGS according to the following empirical laws [21]:

$$E_g = 1.06 + 0.39238x + 0.24762x^2 \tag{3}$$

Material properties	ZnS
Melting point (K)	2038 (WZ, 150 atm)
Band gap E_g at 300 K (eV) (ZB/WZ)	3.68/3.911
Electrical susceptibility (eV)	3.9-4.5
Lattice parameter (ZB) a0 at 300 K (nm)	0.541
ZB structure density at 300 K (g/cm-3)	4.11
Lattice parameters (WZ) at 300 K (nm) a0 = b0 c0 c0/a0	0.3811 0.6234 1.602
WZ structure density at 300 K (g/cm-3)	3.98
Heat capacity Cp (Cal/mol K)	11
Relative dielectric constant ε_r	8.3
Refractive index (ZB/WZ)	2.368/2.378
Absorption coefficient	≤0.15
Electron effective mass (m*/m$_0$)	−0.4
Electrons mobility at 300 K (cm2/V. s)	165
Holes mobility at 300 K (cm2/V. s)	5

Table 2.
Properties of zinc sulfide ZnS [22].

$$\chi_e = 4.6 - 1.15667x + 0.03333x^2 \qquad (4)$$

The choice of the value of E_g (and therefore of χ_e) depends on several factors.

The best yields are obtained with a value of the band gap E_g of about 1.2 eV. This corresponds to a Gallium concentration level close to [Ga] = 30%. This is the value that will be considered in this study.

- **Rear contact: Molybdenum (Mo)**

The back contact here is a thin layer of Molybdenum (Mo) which is 300 nm thick (the standard thickness is between 0.3-1 micron). It has the ability to form ohmic contact with CIGSe [23]. Indeed, Mo can react with selenium (Se) during the deposition of CIGSe to form MoSe$_2$. Consequently, the CIGSe/Mo structure then becomes *CIGSe/MoSe$_2$/Mo* with a thickness of MoSe$_2$ of about 10 nm. MoSe$_2$ is a semiconductor with a gap of 1.41 eV and its existence has the effect of giving an ohmic behavior to the CIGSe/Mo hetero-contact, while reducing recombination at the interface.

- **Substrate: Soda-lime glass**

The standard substrate used to make CIGSe cells is soda lime glass. It's benefit effects were described above in §2.2. Its thickness varies from 1 to 3 mm.

3.1.4 Investigations on the ZnS – Cu (In, Ga) Se$_2$ interface: Highlighting of the surface defect layer (SDL)

Between the ZnS and the absorber, a layer called OVC (Ordered Vacancy Compound) has been identified. Investigations carried out within recent works identify his properties and found that they were similar to that of a Surface Defects Layer (SDL). Ouédraogo et al. [24] and Tchangnwa et al. [25, 26], highlighted the beneficial effect related to the existence of the SDL on cell performance. In fact, the presence of an Indium-enrich micro-layer which exhibits an N-type conductivity (N-SDL), at the top of the P-type conductivity CIGSe material, is responsible of the existence of that defect state layer. That leads to a discontinuity at the band gap level at the interface. It has a positive effect since it enhance the transport of the charge carriers through the junction. Another interpretation is given for the existence of that defect state layer from other authors [27], that is, it results from a copper-poor film at the top of the CIGSe material. Both interpretations complete each other, since the N-SDL is almost located within the CIGSe layer, but exhibits different opto-electrical, electronic and structural properties. As a consequence, at the P-N interface between the N-type ZnS and the P-type CIGSe materials, an homojunction is formed. That is, the N-type SDL is almost fully integrated within the CIGSe structure. That explains why in our structure, we will model our P-N heterojunction (the ZnS-CIGSe junction) as two different interfaces: the ZnS/SDL interface and SDL/CIGSe interface, each of them exhibiting different properties.

3.2 General principle

3.2.1 Mechanism of photovoltaic conversion

The photovoltaic effect is based on the properties of semiconductor materials. Indeed, the latter are capable of absorbing photons of frequency ν whose energy is:

$$\left[E_{photon} = h\nu - E_g\right] \geq \left[E_g = E_C - E_V\right] \tag{5}$$

Where E_g is the value of the forbidden band, E_C and E_V are respectively the energy values of the conduction band and the valence band of the illuminated material.

A semiconductor material alone cannot generate electric current. In order to generate the electric current, one must assemble two semiconductors of different types, thus creating a P-N junction [21]. In this chapter, let consider the denomination heterojunction because the constituent materials of our two semiconductors are different. The P-doped zone is that containing the CIGSe, and the N-doped zone groups together the buffer layer (ZnS) and the window layers (i-ZnO, ZnO: B). During contact between the P and N zones, the majority carriers of each diffuse through the contact surface, at this time a depletion zone is created, positively charged on the side of the N-type semiconductor and a negatively charged zone on the P-type semiconductor side. This transition zone is called the Space Charge Zone (ZCE). The Fermi levels of the two zones equalize, causing the band diagram to bend, introducing a potential barrier V_e at the interface.

The concentration gradient of the majority carriers induces the presence of a permanent electric field in this ZCE at equilibrium. The electric field thus created leads each type of carrier towards the zone where it is the majority carrier (the electrons towards the N zone and the holes towards the P zone). It follows the mechanism of the collection of each majority carrier.

3.2.2 Densities of states and concentrations of charge carriers

Electrons and holes obey the Fermi-Dirac statistic, the probability that an energy level E is occupied by a charge carrier is given by:

$$f_{FD}(E) = \frac{1}{1 + \exp\left(\frac{E - E_f}{K_b T}\right)} \tag{6}$$

Assuming we are in non-degenerate states of energies we have $(E - E_f)/K_b T \gg 1$ and $f_{FD}(E) \rightarrow \exp - \left(\frac{E - E_f}{K_b T}\right)$.

The densities of electrons and holes in the conduction and valence band respectively are given by the following integrals [28].

$$n = \int_{E_C}^{\infty} N(E)f(E)dE = f_{FD}(E_c) = N_c \exp - \left(\frac{E_c - E_f}{K_b T}\right) \tag{7}$$

$$p = \int_{-\infty}^{E_V} N(E)\left(1 - f(E)dE = f_{FD}(E_V) = N_v \exp\left(\frac{E_V - E_f}{K_b T}\right) \tag{8}$$

With:

$$N_C = \frac{2\left(2\pi m_e^* KT\right)^{3/2}}{\hbar^3} \tag{9}$$

and

$$N_V = \frac{2\left(2\pi m_h^* KT\right)^{3/2}}{\hbar^{3.}} \tag{10}$$

The fermi level energy is given by:

$$E_F = \frac{E_C + E_V}{2} + \frac{KT}{2} \ln \left(\frac{N_V}{N_C}\right) = \frac{E_C + E_V}{2} + \frac{KT}{2} \ln \left(\frac{m_h^*}{m_e^*}\right)^{\frac{3}{2}} \tag{11}$$

with: $m_e^* = 0.4 m_e$ and $m_h^* = 1.7 m_e$

3.2.3 Current generation

These are the Poisson equation in the presence of an electric potential φ, and the continuity equations of electrons and holes with well-specified boundary conditions [23].

The Poisson equation for semiconductors is:

$$\frac{d}{dx}\left(\varepsilon \frac{d\varphi}{dx}\right) = -q\left(p - n + N_D^+ - N_A^-\right) \tag{12}$$

The continuity equations for electrons and holes are:

$$\frac{d}{dx}(J_n) = q(R - G) + q\frac{\partial n}{\partial t}; \tag{13}$$

$$\frac{d}{dx}(J_p) = -q(R - G) + q\frac{\partial p}{\partial t} \tag{14}$$

ε is the dielectric constant of the material, φ is the electrostatic potential, n and p are respectively the concentration of free carriers for electrons and holes, N_D^+ and N_A^- are the densities of ionized donors and acceptors, J_n and J_p are the current densities due to electrons and holes. R and G are the rates of recombination and generation of electron-hole pairs, respectively.

$$J_n = q\mu_e n \nabla\varphi + qD_e \nabla n; \tag{15}$$

$$J_p = q\mu_p p \nabla\varphi + qD_p \nabla p \tag{16}$$

The current density in the cell can be written in the following form: (17)

$$J = J_{G\acute{e}neration} - J_{Recombinaison} = -q \int_{-d}^{W+L} G_L(\lambda, x)dx - J_{ir} + q \int_{0}^{W+L} R(x)dx \tag{17}$$

Where G_L is the generation function, J_{ir} is the recombination current at the interface, R is the recombination function in the volume of the absorbent layer. d, W and L are the widths of the buffer layer, ZCE and ZQN respectively [23].

The rate of generation of electron-hole pairs at one dimension of the surface of the semiconductor is given by:

$$G_L(\lambda, x) = \alpha_1(\lambda)F(\lambda)(1 - R(\lambda)) \exp(-\alpha_1 x) \tag{18}$$

$\alpha_1 (\lambda)$ is the number of incident photons per cm^2 per s per unit wavelength. $R(\lambda)$ is the fraction of photons reflected from the surface, α_1 is the absorption coefficient in the semiconductor.

3.3 Study of the performance reduction mechanisms within the device

Some micro-activities took place within the junction when the two materials (ZnS and CIGSe) are gathered together and are submitted to an external electric field and light. These activities which tend to reduce the global performances of the device, are the recombination mechanisms of the photo-generated electron-hole pairs. To recall what we said in **Section 1**, the first challenge of the current researches in the field of solar energy harvesting is the reduction of the quantities of materials while keeping the device performance or enhancing them. This is a great challenge since, the effects of the defect states, which inevitably appear with the reduction of thicknesses, have very detrimental effects on the performance of the cell.

3.3.1 Charge carrier's recombination mechanisms

These mechanisms are characterized by their rates R which describes the number of recombination per unit time and per unit volume of the material and by the lifetime of the charge carriers. There are three of them, but let us just consider the radiative and the Auger recombination.

• **Radiative recombination**

It takes place by the direct transition of an electron from the conduction band to the valence band. The energy of the transition is released as a photon. If the trap levels created by defect states are close to the middle of the forbidden band, the rate of radiative recombination and the lifetime of electron can be given by [21]:

$$R_R \approx \frac{n - n_0}{\tau_{R,n}} \qquad (19)$$

with

$$\tau_{R,n} = \frac{1}{p_0 C_r} \qquad (20)$$

and,
$\tau_{Rad,n}$ is the lifetime of the electrons, C_r is the radiative recombination coefficient, p_0 the hole density at equilibrium.

However, this mechanism is not always so harmful on the performance of the cell because in fact, it is possible that the photon released during this mechanism is reabsorbed and thus forming another electron-hole pair. Indeed, the energy value of the emitted photon is close to that of the band gap.

• **Auger recombination**

These are direct carrier band-to-band transfers. It could be an electron or a hole. However, instead of being emitted as a photon, the energy is transferred to another carrier of the same type as thermal energy. The latter will return to its initial state by interacting with the crystal lattice, it will therefore emit a phonon [21]. The rate of radiative recombination can be given by:

$$R_A \approx \frac{n - n_0}{\tau_{A,n}} \qquad (21)$$

with

$$\tau_{A,n} \approx \frac{1}{p_0^2 C_p} \tag{22}$$

$\tau_{A,n}$ is the lifetime of the electrons, p_0 the hole density at equilibrium, C_p is the Auger recombination coefficient.

We recall these mathematical expressions to highlight the influence of doping process on recombination mechanism rate at a certain point. We will more explain it a little further in the third section.

3.3.2 Investigations on the effects of defect states on cell performances

Most of the time, defect states are a result of the way the processes of preparation or deposition of layer sheets are performed. They act on material properties, mainly on material electrical properties the same way as for adding impurities. Generally, the main goal is to improve charge carriers transport within the material or to reduce recombination mechanism rate. However, as we will see a little further, they have detrimental effects on the cell performances. Recalling what has been said in **§3.1.6**, and because of the highlighted SDL, at the heterojunction level, we will investigate these effects on two interfaces: ZnS/SDL and /CIGSe.

- **Investigation on the ZnS/SDL sub-heterojunction.**

In the **§3.1.5**, we highlighted one of the numerous positive roles of the ZnS on enhancing the global cell performance, that is "it protects the surface of the absorber during the deposition of the ZnO layer, which can cause defects on the surface of the CIGSe". Therefore, a good choice of the deposition process can significantly reduce these defects density at ZnS/SDL sub-heterojunction. If we consider an ideal case, where the preparation and the deposition processes are perfect, that means with no defect reported within the sub-heterojunction, then we may have this situation:

- The negative charges concentration located in the Space Charge Region (SCR), that is almost localized within the top film part of the CIGSe layer is compensated with the positive charges concentration on the other side, resulting from top to bottom of ZnO: B, i-ZnO and ZnS materials.

That is, at equilibrium, it can be described by the following equation:

$$Q_n + qt_{i-ZnO}N_w + qt_{ZnS}N_b = qN_a t_{SCR} \tag{23}$$

where Q_n is the surface charge in the depletion zone of the boron-doped ZnO window layer, q is the elementary charge, N_w, N_b and N_a are the doping concentrations in the i-ZnO, ZnS and CIGSe top film part layers with respective thicknesses t_{i-ZnO}; t_{ZnS} and t_{SCR}.

Introducing a defect state within a material crystallographic structure, is generally materialized by adding a negative charge. Let say, this situation happens at the ZnS/SDL sub-heterojunction section, to compensate the negative charge added due to defect states, we should reduce the width of the SCR in the CIGSe top film part. That action we will increase the recombination rate at the ZnS-SDL level and negatively affect the cell output parameters. This interpretation is confirmed by previous work reports [27].

Worker reference	Subject of study	Reports
[27]	Excess defect at the CdS/CIGS interface solar cells.	Considering a density of defect of $10^{12}cm^2$, and an electron-hole capture section through the interface of $10^{-12}cm^{-2}$, the yield decreases from 18.9-14%.
[29]	Effects of defect states on the performance of CuInGaSe$_2$ solar cells.	For a defect state density of less than $10^{14}cm^{-3}$, in the CIGSe material and not more than $10^{18}cm^{-3}$, in the CdS material, the detrimental effects of defect states are not really perceived.

Table 3.
Reports of recent studies on the effect of defect states on the cell performances.

- **Investigation on the SDL/CIGSe sub-heterojunction**.

Recent studies were carried out on the effects of the density of defect states on the global performance of CIGSe/CdS-based solar cells and their conclusions are summarized within the **Table 3** above [27, 29].

3.4 Modeling and calculation tools

We have modeled our solar cell device by using the version 3.3 of the one-dimensional numerical simulation software SCAPS-1 D^2 [30].

4. Results and discussion

4.1 Optimal value of ZnS electronic affinity

Considering the electrical susceptibility of Zinc Sulfide (χ_e), within the range of 3.9 [31] and 4.5 [32], we investigate the effects of his value on the performance of our modeled device. Observations are mainly carried out on Fill Factor (FF) and Efficiency (η) and for a thickness of the absorber layer of 0.5 μm. The results obtained are plotted in **Figure 2** above.

It shows that the optimum value of the ZnS electrical susceptibility for recording the best performance of our solar cell is defined for χ_e [4.1; 4.5eV]. This result is in very good agreement with those reported in literature [17, 19]. The maximum of the parameters is obtained for $\chi_e = 4.3eV$. This value can be registered as the optimum value of the electrical susceptibility of ZnS for this structure of solar cell.

4.2 Influence of the doping concentration of the CIGSe layer on the performance of the cell

Recent works with the CdS as buffer layer [3] has shown that, beyond a concentration of holes $N_A = 0.8\ 10^{14}cm^{-3}$, the overall parameters of the cell degrade considerably. Ouédraogo et al. [19] have shown in their work that beyond $N_A = 10^{16}cm^{-3}$ the voltage reaches saturation independently of the thickness of the absorber layer. The resulted obtained are plotted on the **Figure 3** below. From these plots, we can see that, varying N_A influences the performances of the cell. For a fixe value of t_{CIGSe}, V_{OC}, increases significantly with the increase of N_A. If we decide as well to increase t_{CIGSe},

---

^{2} SCAPS-1D: Solar Cell Capacitance Simulator in One Dimension. Free software developed by M. Burgelman, Nollet and Degrave from the University of Gent in Belgium in 2000.
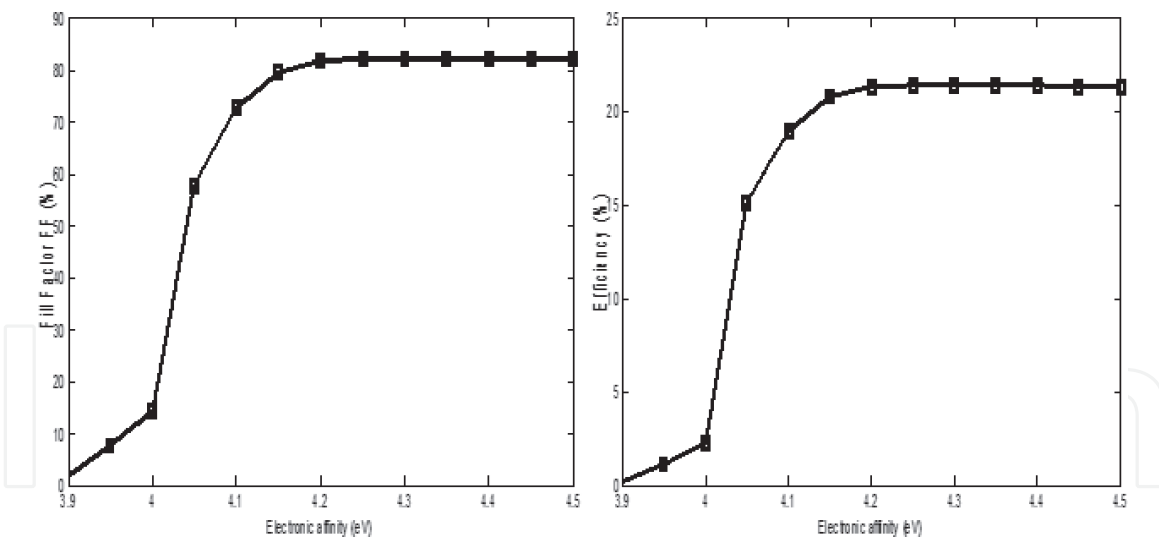
Figure 2.
Influence of ZnS χ_e, on the fill factor (FF) and efficiency.

then for the same value of N_A, V_{OC} will increase. This observation is the same with efficiency (**Figure 3(d)**). Conversely, J_{SC} (**Figure 3(b)**) and the fill factor (FF) (**Figure 3(c)**) decrease significantly with the increase of N_A. By setting the value of N_A, and by varying t_{ZnS}, the output parameters of the cell are almost constant. When the thickness of the absorber layer is less than 250 nm, the performances of the cell are not influenced with variation of N_A in particular FF and η.

But a significant increase on the output results is observed for a doping level $N_A = 10^{15} cm^{-3}$ and with a thickness of the absorber layer no more than 0.5 μm. For $N_A \in \left[10^{14} : 10^{15} cm^{-3} \right]$, and for $t_{CIGSe} < 2500$ nm, the parameters of the cell are globally interesting because $V_{OC} < V_{SAT}$ (**Figure 3(a)**), where V_{SAT} is the saturation voltage of our device. In addition, the short-circuit current is at its maximum value $J_{SC} = J_{(SC)max}$ (**Figure 3(b)**) and the values of the fill factor (**Figure 3(c)**) $FF \approx 85\%$. This observation is important because it will allow to circumscribe the optimal value of N_A. For $N_A > 10^{15}$, the overall performance of the cell increases significantly. Believing that the best performances can be obtained with a high level of intrinsic doping recorded in the absorber layer is an utopia; two factors limit that way of thinking: The quality factor in **Figure 5(c)** decreases significantly and characterizes the poor quality and instability of the solar device in question; For $N_A = 10^{16} cm^{-3}$ and considering $t_{CIGSe} > 500$ nm, saturation is automatically reached. Thus, for $t_{CIGSe} = 500 nm$, we have $V_{(OC)SAT} = 0.8V$; $J_{SC} = 34.39 \, mA/cm^2$, $\eta = 22.27\%$, and $FF = 79.47\%$. let us recall the mathematical expressions given in §3.3.1, those are Eq. (20) and Eq. (22). According to Eq. (20), when we add the holes density P, the lifetime of negative charge carriers decreases since the latter is inversely proportional to hole concentration and to the square root of hole concentration (Eq. (22)). As a conclusion, the benefits of higher doping for P-type conductivity materials are limited by the Auger and radiative mechanisms. Moreover, for $N_A \in \left[10^{15} : 4.10^{15} cm^{-3} \right]$ the performances of the cell are globally very interesting. This would probably justify why Daouda et al. [23] obtained a good yield (18.6%) by working with $N_A = 7.10^{15} cm^{-3}$. However, they quickly reached saturation as soon as $t_{CIGSe} > 1000$ nm. The analysis of the different graphs shows that the optimal intrinsic doping level of CIGSe is $N_A = 10^{15} cm^{-3}$.

$$(V_{oc,ZCE})_{dom} = \frac{E_g}{q} - \frac{nkT}{q} \ln \left(\frac{1}{J_{ph}} * \frac{q D_n N_C N_V}{L_n N_A} \right) \qquad (24)$$
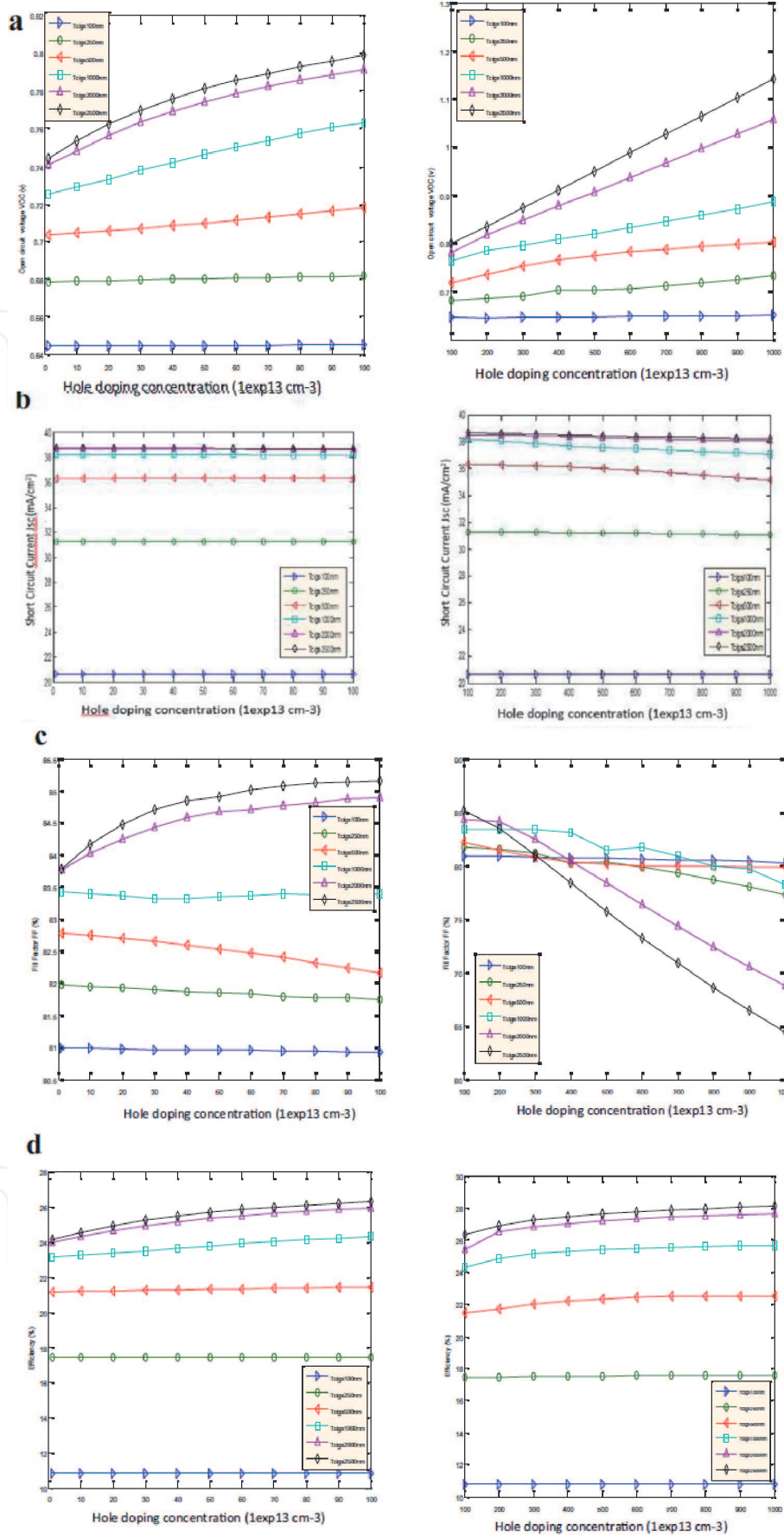
Figure 3.
Influence of the acceptor density N_A on the cell parameters for different CIGSe thickness values. (a) Open circuit voltage (V_{OC}), (b) short-circuit current density (J_{SC}), (c) fill factor (FF), and (d) efficiency (η).

where D_n is the electron scattering coefficient, N_C and N_V the state densities in the conductance and valence bands, L_n the electron scattering length, N_A the density of acceptor states in the CIGSe layer. From this relation when N_A

increases, the voltage $(V_{oc,ZCE})_{dom}$ tends to reach critical value materialized as saturation.

The results obtained are in good agreement with those reported by Ouédraogo and co-workers [23] who were investigating on a CIGSE-based cell structure with CdS as buffer layer. We bring out from these results that both the choice of the buffer layer material and its thickness are not limiting input parameters for hole doping level within the absorber layer. Th high density of recombination mechanisms and a weak collection mechanism of free charge carriers can explain very well the decreasing of short-circuit current (J_{SC}). For a doping level of more than 10^{15} cm^{-3}, within the CIGSe material, the output parameters of our device are not enhanced.

4.3 Effects of the thickness of CIGSe on cell performance

In this subsection, we are investigating how the global output parameters of the device is affected when the thickness of the active layer is a variable. The simulations are carried considering the optimized properties of the other layers. From literature, the commonly used thickness for absorber layer is within the range [2000: 3000 nm]. Since we are on the way of reducing materials quantities, we will observe the performances of our cell with CIGSe thickness ranged from 100 nm to 3000 nm.

There are two main areas of interpretation,

- the first for 100 $nm < t_{CIGSe} < 500$ nm, and

- the second for 500 $nm < t_{CIGSe} < 2500$ nm.

Vital information came out from the results obtained. The global performances of the cell (J_{SC}, V_{OC}, FF, η) are improved significantly when the thickness of the absorber layer t_{CIGSe} is gradually increased.J_{SC} is the most sensible parameter, the values of $20.65 mA/Cm^2$ and $30.31 mA/Cm^2$ are recorded for t_{CIGSe} values of 100 nm and 500 nm respectively. That is a jump of about $16 mA/Cm^2$ (**Figure 4(b)**). In fact, at the absorber and Molybdenum junction, the rate of backward recombination mechanisms are reduced significantly because of the Space Charge Region which is completely localized within the active material layer. A similar situation is observed with the plot of the open-circuit voltage, which value increases from 0.65 V for 100 nm of absorber thickness, to 0.76 V for 1000 nm of thickness respectively. That is a gain of 0.13 V! (**Figure 4(a)**). That is not all, the efficiency increased from 10.78% to 24.31%, a jump of almost 14% (**Figure 4(d)**). A value of 83.4% was recorded for the Fill Factor (**Figure 4(c)**). Those results are just impressive. Let us remember that we are undertaking our calculations based on optimized values of properties of the other materials that constitute our structure. These are reported in the **Table 4** below.

For a thickness of the absorber layer between 500 nm and 2500 nm, we record very good value of our cell output performance. Of course, for a thicker CIGSe layer, the probability of absorbing a wide range of light Spectrum is higher and thus, and since the materials properties have been optimized, the quantum efficiency will be higher too. From **Figure 4(a)**, we can easily notice how remarkably V_{OC} increases with absorber layer thickness.

Pogrebjak and co-workers [7, 32] who worked on the influence of temperature on CIGSe-based ultra-thin solar cells and on nano-scale technologies, obtained results which are in good agreement with those obtain during our simulations. The slight difference in results can be explained by global condition of calculation such
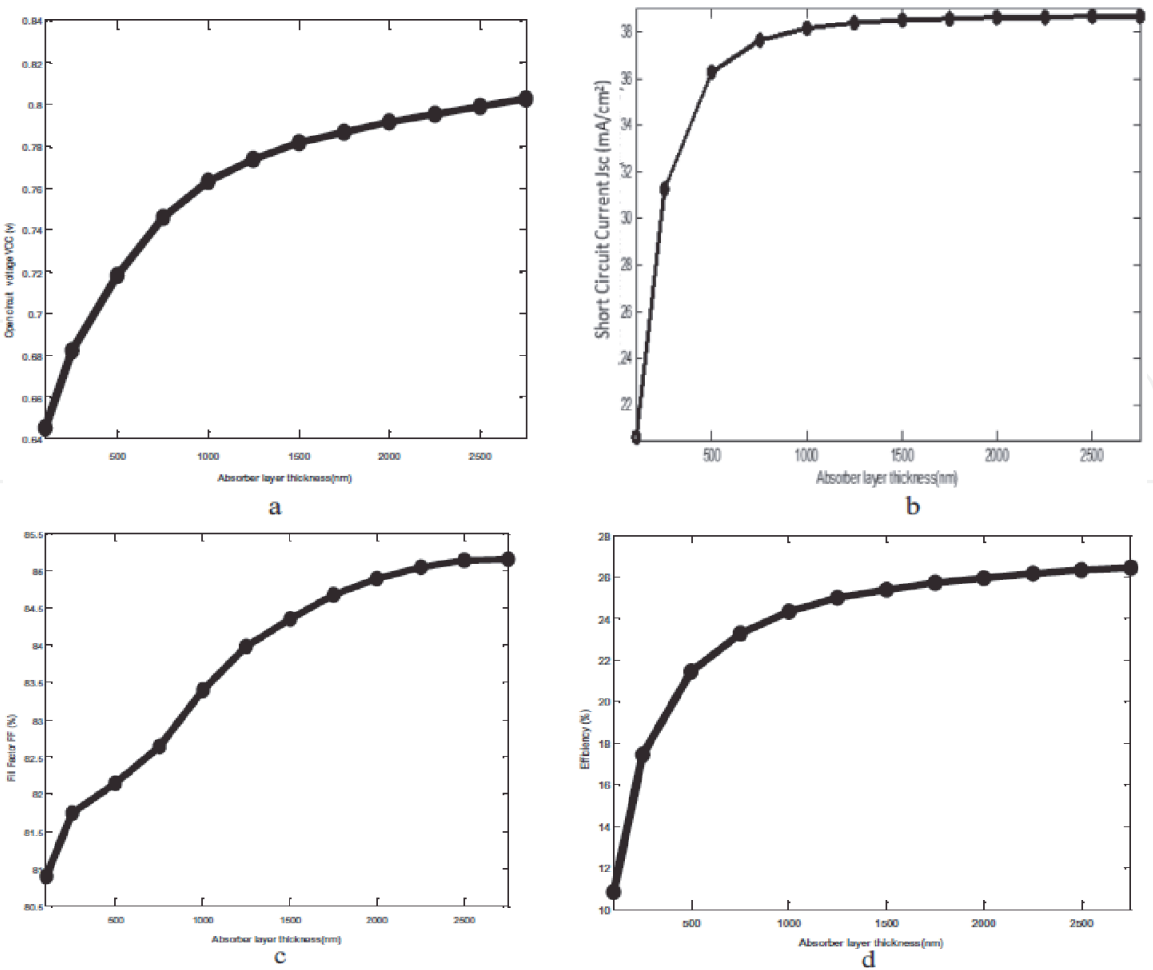
Figure 4.
Influence of the thickness of the absorber layer on the output parameters of the cell for $t_{ZnS} = 5$ nm $N_A = 10^{15} cm^{-3}$. (a) Open circuit voltage (V_{OC}), (b) short-circuit current (J_{SC}), (c) fill factor (FF), and (d) efficiency (η).

Material/layer	Optimized properties considering each material			
	Crystallographic structure	Electrical susceptibility	Dielectric constant	Thickness
ZnS	**Zinc Blende**	4.3	8.3	5 nm
	Intrinsic doping level			
Cu (In, Ga) Se₂	$10^{15} cm^{-3}$			
	Assumption on SDL			
Surface defect layer (SDL)	Modeling of SDL properties and splitting it in two sub-interfaces: ZnS/SDL and SDL/CIGSe with different properties			

Table 4.
Optimized value of some layers/interface properties used for simulation.

Absorber layer thickness (nm)	V_{OC} (V)	JSC (mA/cm^{-2})	FF	η
500	0.7180	36.31	82.16%	21.42%
1000	0.7633	38.18	83.39%	24.31%
2500	0.7989	38.66	85.15%	26.30%

Table 5.
Output parameters of our photovoltaic device.

as external temperature, incident light power, and defect states density input values.

Running several calculations allowed us to detect the critical values of some properties values beyond which the device is no more stable, even if the efficiency is higher. This is for example 2750 nm for absorber layer thickness or an intrinsic doping level of more than 10^{15}. Since we manufacture our solar cell device based on the model proposed in this work and watching out not to have these highlighted critical values, our device will definitely work in good condition. The **Table 5** above reports the best performance of our cell obtained during all our calculations.

5. Conclusion

This chapter focused on enhancing efficiencies of solar cell devices working on a CIGSe-based second – generation ultra-thin model, and using Zinc Sulfide (ZnS) as a window layer. Vital information is found when investigating the influence of layers and interfaces properties on output parameters of the device. The challenging part is not the use of the promising ZnS material itself, but it is to find through literature and recent works, the key values of the ZnS properties in a preferential crystallographic orientation, that allow to obtain better performances and also the good choice of materials that make up the other layers. Starting on that point, the following cell *(Ni/Al)/MgF2/ZnO: B/i-ZnO/ZnS/CuInGaSe$_2$/Mo/Substrate* has been modeled and simulations were ran from version 3.3 of the SCAPS-1D software. The benefits associated with the existence of the Surface Defects Layer (SDL) on the device stability have been highlighted. The Blende structure of Zinc Sulfide material (ZnS) forms a more stable lattice matching with CIGSe absorber layer chalcopyrite structure. That is why most of the key values of its intrinsic properties are obtained from that orientation, especially its band gap $E_{g\_ZnS} = 3.68 eV$, its electrical susceptibility $\chi_e = 4.3 eV$, its dielectric constant $\varepsilon_r = 8.3$ according to simulation results. After running numerous simulations, very promising performances are recorded, a conversion efficiency of 26.30% and a fill factor of 85.14%. Going further in research, some may obtain even more interesting results by directing the work towards implementation of additional manufacturing technologies, including the use of antireflective coatings and the texturization of the inner back layers.

Author details

Fridolin Tchangnwa Nya* and Guy Maurel Dzifack Kenfack
Department of Physics, Faculty of Science, University of Maroua, Maroua, Cameroon

*Address all correspondence to: nyafridolin@yahoo.fr

IntechOpen

References

[1] Martin Green A., Keith Emery, Yoshihiro Hishikawa, Wilhelm Warta, Ewan Dunlop D., Dean Levi H. and Anita Ho-Baillie W. Y. Mint: Solar cell efficiency tables (Version 49). Progress in Photovoltaics and applications. 2020. DOI:10.1002/pip.2855.

[2] Mostefaoui M., Mazari H., Khelifi S., Bouraiou A., Dabou R. Mint: Simulation of high efficiency CIGS solar cells with SCAPS-1D software. Elsevier, Energy Procedia 74, 736–744. 2015. https://doi.org/10.1016/j.egypro.2015.07.809.

[3] Tchangnwa Nya F., Touogam Touolak B., Ejuh W. G., Ouédraogo S. and Njaka, J. M. Energy and Environment Focus Vol. 6, pp. 1-9. 2017.

[4] Powalla M., Cemernjak M., Eberhardt J., Kessler F., Kniese R., Mohring H.D., Dimmler B. Mint: Large-area CIGS modules: pilot line production and new developments. Sol. Energy Mater. Sol. 2006. Cells 90, 3158.

[5] Liao D., Rockett A. Mint: Cd doping at the CuInSe2/CdS heterojunction. J. Appl. Phys. 2003. 93, 9380.

[6] Li Z., Yu-Ming X., Chuan-Ming X., Qing H., Fang L.F., Chang-Jian L., Yun, S. Mint: Microstructural characterization of Cu-poor Cu (In,Ga) Se2 surface layer. Thin Solid Films. 2012. 520, 2873.

[7] Pogrebjak A.D., Muhammed A.K.M. Mint: Simulation study of effect operating temperature and layer thickness on thin film CIGS solar cell performance nano and electronic. Physics 3 (3), 2011, 2012. 051–058.

[8] Duchatelet Aurelien. Synthèse de couches minces de Cu (In,Ga)Se2 pour les cellules solaires par électro-dépôt d'oxydes mixtes de cuivre-indium-gallium, Molécules et Matière condensée. [thesis]. Université des Sciences et Technologies de Lille. France; 2013. http://doc.univ-lille1.fr

[9] W. Chen et al. Dans Proc. 19th IEEE Photovoltaic Specialist Conf. 1987.

[10] Eman N. M. Mint: Surface morphology and structural properties of ZnS and ZnS:Al thin films. International journal of Innovative Research in Sciences, Engineering and Technology, Vol. 3, ISSN: 2319-8753. Issued 1, January 2014.

[11] Won Song, Bo-Ra Koo, Seok Eui Choi, Yong-Taeg Oh, and Dong-Chan Shin. Mint: Optical and structural properties of a ZnS buffer layer fabricated with deposition temperature of RF magnetron sputtering system. International Journal of Chemical, Molecular, Nuclear, Materials and Metallurgical Engineering Vol:6, No: 12. 2012.

[12] Wang Cai-Feng, LI Qing-Shan, LV Lei, ZHANG Li-Chun, QI Hong-Xia, CHEN Hou. Mint: Structural, optical and electrical properties of ZnS/porous silicon heterostructures. CHIN.PHYS. LETT, Vol. 24, No. 3 (2007) 825.

[13] Benghabrit S. Elaboration et caractérisation de couches minces CdS par bain chimique CBD pour application photovoltaïque. [thesis]. Université des Sciences et de la Technologie d'Oran. 2015.

[14] Rayan, D.A., Elseman, A.M. & Rashad, M.M. Mint: Remarkable impact of Ni2+ ion on the structural, optical, and magnetic properties of hexagonal wurtzite ZnS nanopowders. Appl. Phys. A 124, 659 (2018). https://doi.org/10.1007/s00339-018-2084-5

[15] Appl. Phys. A 117, 877–890 (2014).

[16] ACS Sustainable Chem. Eng. 2016, 4, 9, 4875–4886.

[17] Pawan Kumar, Aravind Kumar, Dixit P.N. and Sharma T.P. Mint: Optical, structural and electrical properties of ZnS thin film. Indian Journal of pure & applied physics, Vol 44, pp.690-693. September 2006. IPC Code: H01L 27/00.

[18] Zenebe Assefa Tsegaye. Density functional theory studies of electronic and optical properties of ZnS alloyed with Mn and Cr, NTNU-Throndheim, Condensed Matter Physics, Norwegian University of Sciences and Technology. 2012.

[19] Habibah, B. L'effet de la température du substrat et de la molarité sur les propriétés des couches minces de sulfure de zinc déposées par spray ultrasonique. Université Mohamed Kheider-Biskra. 2013.

[20] Platzer-Bjorkman C. Band Alignment Between ZnO-Based and Cu (In,Ga)Se2 Thin Films for High Efficiency Solar Cells. Acta Universitatis Upsaliensis. Digital Comprehensive Summaries of Uppsala Dissertations from the faculty of Sciences and technology 136. 80 pp. Uppsala. 2006. ISBN 91-554-6435-1.

[21] Charles Roger. Développement de cellules photovoltaïques à base de CIGS sur substrats métalliques. HAL archives-ouvertes.fr. [thesis]. Université de Grenoble Alpes. Français. NNT: 2013GRENI050. Tel-00965592. 2013. https://tel.archives-ouvertes.fr/tel-00965592

[22] Kassap S., Capper P. Mint: Springer Handbook of Electronic and Photonic Material. 2007. Url: http://www.springer.com/978-0-387-26059-4.

[23] Daouda O., Bawindsome Kebre M., Zougmoré F., Njomo D., Ouattara F. Mint: Numerical simulation of Cu (In, Ga)Se2 solar cells performances. Jounal of Energy and Power Engineering 9 1047-1055. 2015. doi : 10.17265/1934-8975/2015.12.002.

[24] Ouédraogo S., Zougmoré F. and Njaka J.M. Mint: Numerical Analysis of Copper-Indium-Gallium-Diselenide-based Solar Cells by SCAPS – 1D. Indawi Publishing Corporation, International Journal of Photoenergy, Article ID 421076, 9 pages. 2013. http://dx.doi.org/10.1155/2013/421076

[25] Tchangnwa Nya F., Dzifack Kenfack G. M., Geh Ejuh W., Touogam Touolak B., Ndjaka J. M. Mint: Highlighting some layers properties in performances optimization of CIGSe based solar cells: Case of Cu (In, Ga) Se–ZnS. Journal of King Saud University – Science 31 (2019) 1404–1413 https://doi.org/10.1016/j.jksus.2018.03.026

[26] Touafek, N., Mahamdi, R. Excess defect at the CdS/CIGS interface solar cells. Chalcogenide Lett. 11 (11), 589–596. 2014.

[27] Farhan Rana. Semiconductor Optoelectronics, Chapter 2: Semiconductor Heterostructures. Cornell University. Accessed online March 04, 2017.

[28] Rüdiger Memming Wildbret. Semiconductor Electrochemistry, Second Edition, Edited by, 25462 Rellingen Germany. Published by WILEY-VCH, Germany. 2015.

[29] Wan Fucheng, Tang Fuli, Xue Hongtao, Lu Wenjiang, Feng Yudong, Rui Zhiyuan. Mint: Effects of defect states on the performance of CuInGaSe2 solar cells. J. Semiconductors 35 (2). 2014. DOI:10.1088/1674-4926/35/2/024011

[30] Burgelman M., Nollet P., Degrave S. Mint: Modelling polycrystalline semiconductor solar cells. Thin Solid Films. 2000. 361–362, 527–532.

[31] Al-Ani S.K., Ba-Yashoot A.Kh., Makadsi M.N., Ai-Sharbaty A.M. Photovoltaic properties of n-(ZnS) x (CdTe)1-x/p-Si. 2006.

[32] Ramli H., Kamal S., Abd Rahim T., Muhaimin M. Optimization of Zinc Sulfide (ZnS) electron affinity in Copper Indium Sulfide (CIS) based photovoltaic cell. Chalcogenide Lett. 10 (6), 189–195. 2013